







Unveiling Galactic substructures with M Giant stars: A kinematic and chemical study based on LAMOST DR9, Gaia DR3 and APOGEE DR17

Longfei Ding¹ , Jing Li¹ , Xiang-Xiang Xue^{2,3} , Hao Tian^{2,3} , Zhengzhou Yan¹  and Gang Zhao^{2,5} 

¹ School of Physics and Astronomy, China West Normal University, Nanchong 637002, China;
lijing@shao.ac.cn, zzyan@bao.ac.cn

² National Astronomical Observatories, Chinese Academy of Sciences, Beijing 100101, China;
xuexx@nao.cas.cn

³ Institute for Frontiers in Astronomy and Astrophysics, Beijing Normal University, Beijing 102206, China

⁴ School of Astronomy and Space Science, University of Chinese Academy of Sciences, Beijing 100049, China;

Received 20XX Month Day; accepted 20XX Month Day

Abstract Based on the updated M giant star catalog selected from LAMOST DR9, we identify substructures within the integrals-of-motion space through Friends-of-Friends clustering algorithm. We obtain members belonging to several known substructures: the Sagittarius stream, Galactic Anticenter Substructure (GASS), Gaia-Enceladus-Sausage (GES), Splash, and the high- α disk. Furthermore, we also identify two groups which cannot be clearly associated with previously known substructures. Our findings confirm the existence of metal-rich constituents within the GES, representing newly formed stars that originated from the metal-enriched gas delivered during the GES merger event and subsequently evolved. Additionally, this study further expands the sample of GASS, high- α disk, and Splash stars. Analysis of these metal-rich M giant stars as members of the GES, Splash, and high- α disk components supports an evolution scenario for the early Milky Way, as proposed by previous studies. In this scenario, stars initially formed in a high- α primordial disk were dynamically heated by the massive accretion event (GES). This process redistributed stellar orbits, creating the Splash population, while the undisturbed portion of the primordial disk persisted as the present-day high- α disk component.

Key words: Galaxy: evolution – Galaxy: formation - Galaxy: kinematics and dynamics - Galaxy: disc - Galaxy: halo - Galaxy: structure

1 INTRODUCTION

Galactic archaeology plays a crucial role in uncovering the formation and evolutionary history of the Milky Way (Helmi 2020). According to the Λ CDM model, the Galaxy primarily formed through hierarchical mass assembly, where satellite galaxies merged with the Milky Way (Horta et al. 2023). These events created substructures in the Galactic halo and disk, characterized by stars with consistent kinematic, dynamical, and chemical properties (Helmi 2020). Studying these substructures helps reconstruct the Galaxy’s merger history (Helmi et al. 2018; Massari et al. 2019; Yang et al. 2019a; Myeong et al. 2019; Koppelman et al. 2019a; Bonaca et al. 2020; Li et al. 2021; Zhao & Chen 2021; Wang et al. 2022).

Utilizing data from photometric and spectroscopic surveys, such as the Sloan Digital Sky Survey (SDSS; York et al. 2000; Ahumada et al. 2020), the Two Micron All Sky Survey (2MASS; Skrutskie et al. 2006), Pan-STARRS1 (PS1; Chambers et al. 2016), the Large Sky Area Multi-Object Fiber Spectroscopic Telescope (LAMOST; Zhao et al. 2012; Yan et al. 2022), and Gaia (Gaia Collaboration et al. 2023), more and more substructures have been identified in the Milky Way (Newberg & Carlin 2016; Belokurov et al. 2018; Haywood et al. 2018; Myeong et al. 2018; Ibata et al. 2021; Mateu 2023). Recent studies have used diverse datasets and methods to identify Galactic substructures. For example, using various types of stellar samples such as K giants, BHB stars, and RR Lyrae stars, many substructures within the Galactic halo, including the Sagittarius (Sgr) stream, Gaia-Enceladus-Sausage (GES), Sequoia, Helmi stream, Thamnos and LMS-1, have been identified (Yang et al. 2019b; Yuan et al. 2020; Naidu et al. 2020; Wang et al. 2022; Sun et al. 2024). Meanwhile, applying various methods (such as Friends-of-Friends (FoF), HDBSCAN, StarGO and STREAMFINDER) to sample in phase space¹ and integrals of motion (IoM) space² based on position-velocity information has made the identification of Galactic substructures more accurate and efficient (Belokurov et al. 2020; Necib et al. 2020; Feuillet et al. 2021; Malhan 2022; Rix et al. 2022; Malhan & Rix 2024; Tang et al. 2024; Tian et al. 2024; Zhang et al. 2024).

Yang et al. (2019a) obtained more than 13,000 K-giant stars in the Galactic halo from LAMOST DR5 and Gaia DR2. Using the six-dimensional (6D) position-velocity information (l , b , d , V_{los} , V_l , V_b) and the FoF clustering algorithm, substructures such as the Sgr Stream, Monoceros Ring, Virgo Overdensity, Hercules-Aquila Cloud, and Orphan Stream were identified. Naidu et al. (2020) constructed a sample of 5,684 giant stars in the region $|b| > 40^\circ$ and $d_{\text{helio}} > 3$ kpc from the H3 (“Hectochelle in the Halo at High Resolution”) Survey. Based on stellar properties in the IoM and action spaces, the analysis revealed various components of the Milky Way, including the Sgr Stream, Aleph, High- α Disk, In-situ Halo, GES, Helmi Stream, Thamnos, High-Energy Retrograde Halo (Sequoia, Arjuna, I’itoi), Wukong, and the Metal-Weak Thick Disk (MWTD). Wang et al. (2022) compiled 3,003 ab-type RR Lyrae stars from SDSS DR12, LAMOST DR6, and Gaia EDR3, located in the Galactic halo. Orbital parameters in the IoM space were employed together with the FoF clustering algorithm to identify substructures including the Sgr Stream, GES, Sequoia, Helmi streams, and three additional groups possibly associated with globular clusters NGC 5272, 6656, and 5024. Tang et al. (2024) selected 6,454 FGKM-type halo stars ($T_{\text{eff}} = 3,500\text{--}8,000$ K,

¹ The three-dimensional position and three-dimensional velocity space.

² E is the total energy of the star, L_z is the component of the star’s orbital angular momentum in the vertical direction, and (J_R, J_Φ, J_z) are three actions in an axisymmetric system. All these parameters are integrals of motion (Ollongren 1965; Binney & Tremaine 2008; Binney 2012; Helmi 2020).

$|V - V_{\text{LSR}}| > 210 \text{ km s}^{-1}$) from the medium-resolution data of LAMOST DR9. Using energy and angular momentum information in the IoM space, the HDBSCAN clustering algorithm enabled the identification of GES, Helmi streams, the high- α disk, the in-situ halo, and three additional clusters not clearly linked to known substructures.

While these studies primarily utilized K giants, BHBs, RR Lyrae stars, and other tracers to probe the Galactic halo, M giant stars—with their unique combination of high luminosity and lower susceptibility to interstellar extinction—offer complementary advantages for mapping both distant and low-latitude substructures. M giants are red giant branch (RGB) stars with low temperature and high luminosity (Li et al. 2023). On the one hand, the high luminosity allows them to be used to trace the distant volumes, which are in the Galactic halo. On the other hand, the lower temperature indicates that most of the flux is distributed at the long wavelength, which makes the M giants suffer lower susceptibility to extinction. This provides an opportunity to study the outer volumes of the disk with low latitude (Qiu et al. 2023).

Li et al. (2019) obtained an M giant star sample with complete phase-space information by combining LAMOST DR4 spectroscopic data, ALLWISE photometry, and accurate proper motions from Gaia DR2. Based on the typical kinematic properties of the Sgr stream, they selected 164 pure Sgr stream M giant stars. In the same year, Yang et al. (2019b) obtained a large sample of M giants, K giants, and BHB stars by combining data from LAMOST DR5, SEGUE-2, 2MASS, and WISE. Using the FoF clustering algorithm in IoM space, they identified more than 3,000 candidate stars of the Sgr stream and provided a detailed characterization of their kinematic and chemical properties. Based on the spectroscopic data from LAMOST DR5 and the precise proper motions from Gaia DR2, Li et al. (2021) applied the same method and identified 280 M giant candidates belonging to an anti-Galactic center substructure in the low-latitude region. These studies demonstrated the potential of M giants in tracing distant and low-latitude Galactic features.

The LAMOST DR9 catalog, with its expanded sample of 58,076 M-giant stars (Li et al. 2023; Qiu et al. 2023), provides a valuable resource for exploring substructures in the Galactic halo and disk. By combining Gaia DR3 data and applying FoF clustering methods in IoM space, we aim to identify substructures and study their properties.

This paper is organized as follows. Section 2 describes the M giant sample used in this study. Section 3 introduces the methods employed to identify substructures. In Section 4, we present the substructures identified through clustering and their characteristics. Finally, the discussion and conclusion are presented in Section 5.

2 DATA

In this work, we use the M giant sample from Li et al. (2023) to investigate Galactic substructures. Based on the low-resolution spectra of LAMOST DR9, Li et al. (2023) selected a reliable sample of 58,076 M giant stars and determined their radial velocities using the cross-correlation-based *laspec* algorithm (Zhang et al. 2021). The velocity offset and dispersion relative to Gaia DR3 and APOGEE DR17 are approximately 1 km s^{-1} and 4.6 km s^{-1} , respectively. Based on this dataset, Qiu et al. (2023) constrained the K-band absolute magnitude to estimate distances for the sample, achieving a relative statistical uncertainty of approximately 25%.

Combining the above data with precise proper motions provided by Gaia DR3 (Gaia Collaboration et al. 2023), we construct a catalog of 43,923 M giant stars, including their right ascension (R.A.), declination (Dec.), distances, radial velocities, and proper motions. Additionally, to investigate the origins of the substructures, we incorporate $[M/H]$ and $[\alpha/M]$ parameters by cross-matching with APOGEE DR17 (Abdurro’uf et al. 2022).

This work adopts both a Galactocentric Cartesian coordinate system (X, Y, Z) and a Galactocentric spherical coordinate system (r, θ, ϕ) , where the positive direction of V_ϕ is opposite to the rotation of Galactic disk. Using the Sun’s position of $(-8, 0, 0)$ kpc (Reid 1993), the solar motion of $(11.1, 12.24, 7.25)$ km s^{-1} (Schönrich et al. 2010) and the local standard of rest velocity of 220 km s^{-1} (Kerr & Lynden-Bell 1986), we calculate the three-dimensional positions (X_{gc}, Y_{gc}, Z_{gc}) and velocities (U, V, W) of all M giant stars in the Cartesian coordinate system, as well as the velocities (V_r, V_θ, V_ϕ) in the spherical coordinate system.

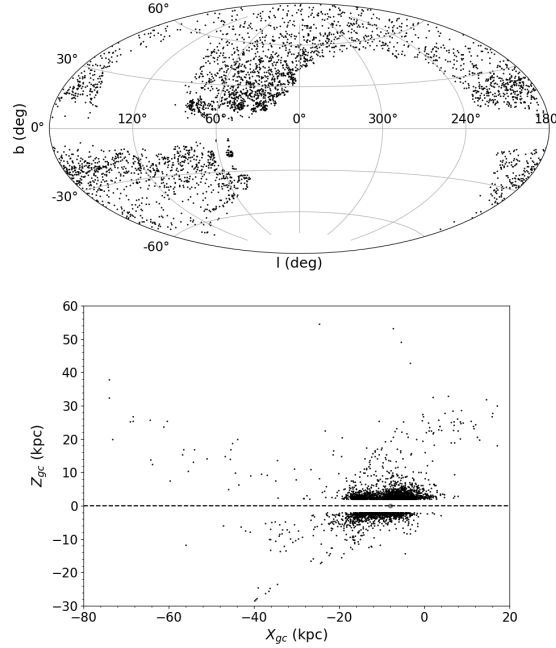


Figure 1. The distribution of the selected M giant sample in phase space: Galactic coordinates (l, b) (upper panel) and $X_{gc} - Z_{gc}$ plane (lower panel).

Considering the substantial number of disk stars in our sample, to minimize the impact of the thin disk and thick disk, we only include samples with $|Z_{gc}| > 2$ kpc in the clustering analysis. In future work, we will further analyze the M giant sample with $|Z_{gc}| < 2$ kpc. Additionally, to ensure data reliability, we retain only stars with a total velocity $V_{\text{tot}} = \sqrt{U^2 + V^2 + W^2}$ less than 400 km s^{-1} , and velocity component uncertainties σ_U , σ_V , and σ_W all smaller than 100 km s^{-1} . As a result, the final sample used for identifying substructures consists of 3,343 M giant stars. The parameters of these stars are listed in Table 1. Figure 1 shows the spatial distribution of the sample in the Galactic coordinate system and the $X_{gc}-Z_{gc}$ plane. Furthermore, the velocity distributions (V_r, V_ϕ, V_θ) and the metallicity distributions are shown in Figure 2. Since M giants lack reliable chemical abundance parameters, we used K giants from Yang et al.

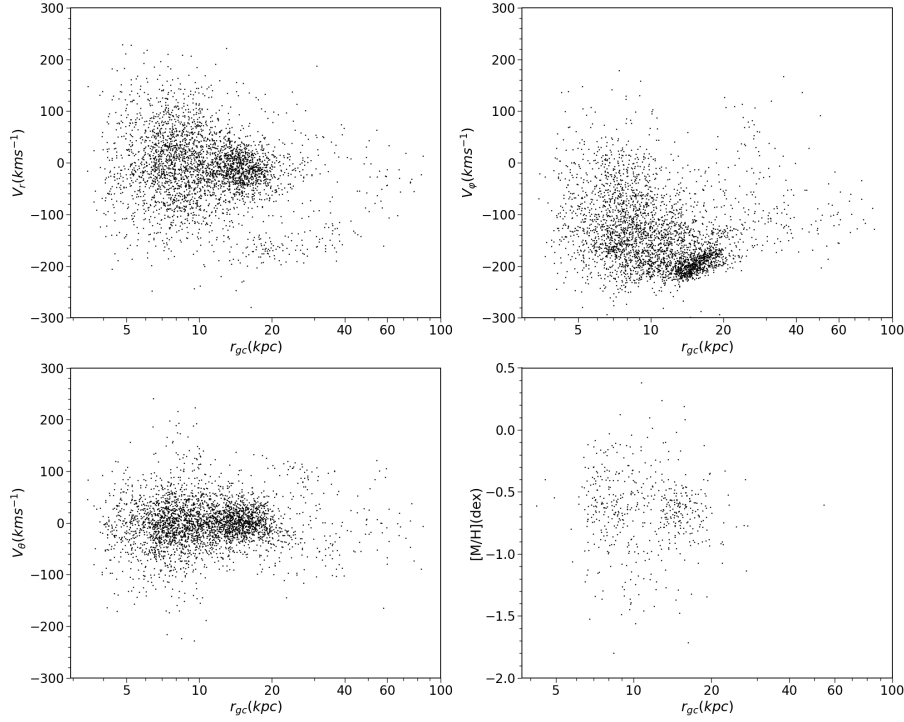


Figure 2. The distribution of the selected M giant sample’s velocities (V_r , V_ϕ , V_θ) and $[M/H]$ relative to the Galactocentric distance (r_{gc}).

(2019b) as the disk star sample. These stars were cross-matched with APOGEE DR17 to derive $[M/H]$ and $[\alpha/M]$ for comparison with the substructures.

Table 1. Parameters of all M giant stars used for identifying Galactic substructures.

LAMOST	Gaia	APOGEE	R.A.	Dec.	d	d _{err}	rv	rv _{err}	pmra	pmra _{err}	pmdec	pmdec _{err}	$[M/H]^a$	$[M/H]_{err}$	$[\alpha/M]^a$	$[\alpha/M]_{err}$
783703241	6.02087E+17	2M08413271+1143476	130.386	11.7299	4.83058802	0.74150176	68.94289	0.10528198	-1.041	0.021	0.354	0.016	-0.55591	0.008231559	0.107612	0.00657604
158703190	2.66032E+18	-	351.848	4.87693	2.53512863	0.389145655	-76.3728	0.10636841	8.169	0.018	-8.97	0.013	-	-	-	-
397903189	1.56292E+18	2M13232252+5232106	200.844	52.5362	2.398832919	0.36822408	-85.57615	0.15323456	-0.504	0.016	-4.96	0.021	-0.74163	0.008905697	0.261675	0.007471177
882612040	3.739E+18	-	203.599	12.3667	2.558585887	0.392746376	-6.612488	0.10685303	1.117	0.036	-16.564	0.018	-	-	-	-
397804118	8.4228E+17	2M11070958+5208002	166.79	52.1334	2.582260191	0.396380413	-76.66522	0.14766236	0.33	0.012	-2.414	0.011	-0.60106	0.008349871	0.123219	0.006826421
841612098	2.56403E+18	-	17.3769	4.64255	2.779713268	0.426689726	-34.434998	0.11698608	3.149	0.027	-6.372	0.018	-	-	-	-
903102026	3.86886E+18	-	160.988	8.68141	2.60615355	0.400048076	19.425537	0.113559574	-5.642	0.018	1.054	0.016	-	-	-	-
906510249	1.44416E+18	2M13503093+2433256	207.629	24.5571	2.60615355	0.400048076	-32.06021	0.10935791	0.231	0.034	-0.869	0.025	-0.32153	0.0077390824	0.092155	0.005329758
782303210	6.02275E+17	2M08432673+1239418	130.861	12.6616	5.152286446	0.790882901	15.706909	0.17940918	0.933	0.016	-5.709	0.012	-1.2221	0.010783301	0.15455501	0.010562286
442215130	1.51355E+18	-	190.663	31.3892	2.937649652	0.450933173	-11.605164	0.1572583	-11.118	0.024	-8.402	0.025	-	-	-	-

Notes.

^a $[M/H]$ and $[\alpha/M]$ from APOGEE DR17.

(This table is available in its entirety in machine-readable form.)

3 METHOD

Over its evolutionary history, particularly in the first three billion years, the Milky Way has undergone multiple mergers with dwarf galaxies. Dynamical theory predicts that, despite the loss of spatial coherence from dynamical mixing, orbital characteristics persist in IoM space. This preservation offers a promising approach to trace the properties of their progenitor systems (Roederer et al. 2018; Massari et al. 2019; Koppelman et al. 2019b; Malhan 2022; Malhan & Rix 2024; Xue et al. 2024, in preparation). Recent studies (e.g., Yang et al. 2019b; Koppelman et al. 2019a; Naidu et al. 2020; Li et al. 2021; Wang et al. 2022; Tang

et al. 2024; Zhang et al. 2024; Sun et al. 2024) have demonstrated the feasibility of identifying substructures in IoM space.

In a spherical potential without considering dynamic friction, Xue et al. (2024, in preparation) defined five IoM parameters: (ec , a , l_{orbit} , b_{orbit} , l_{apo}) (Yang et al. 2019b; Li et al. 2021; Wang et al. 2022). The definitions of the parameters are as follows:

- **Orbital eccentricity** ec : $ec = \frac{r_{\text{apo}} - r_{\text{per}}}{r_{\text{apo}} + r_{\text{per}}}$,
- **Semi-major axis** a : $a = \frac{r_{\text{apo}} + r_{\text{per}}}{2}$,
- **Orbital pole direction** (l_{orbit} , b_{orbit}): $l_{\text{orbit}} = \arctan\left(\frac{L_y}{L_x}\right)$ and $b_{\text{orbit}} = \arcsin\left(\frac{L_z}{L}\right)$,
- **Apocenter direction** l_{apo} : the angle between the apocenter and the projection of the x -axis on the orbital plane.

To quantify the orbital separations between stars, we define the orbit-likelihood distance δ_{ij} following Wang et al. (2022):

$$\delta_{ij}^2 = \omega_\theta \theta_{ij}^2 + \omega_{\Delta a} (a_i - a_j)^2 + \omega_{\Delta e} (e_i - e_j)^2 + \omega_{\Delta l_{\text{apo}}} (l_{\text{apo},i} - l_{\text{apo},j})^2 \quad (1)$$

Here, ω_θ , $\omega_{\Delta a}$, $\omega_{\Delta e}$, and $\omega_{\Delta l_{\text{apo}}}$ are normalization weights (see Wang et al. 2022 for details). The FoF algorithm is employed for substructure identification. In the FoF algorithm, two stars are linked into a group if their orbit-likelihood distance δ is smaller than a specified threshold (linking length). Stars are subsequently added to the group if δ between them and any group member is smaller than the linking length. This process is iterated until no more stars can be added to the group. At this point, the group construction is complete (Wang et al. 2022; Sun et al. 2024).

To ensure that the members of each substructure are identified as completely as possible and obtain reliable clustering results, we set the linking length range from 0.138 to 0.487 and only retain groups containing more than 10 members. Details of the linking length selection are provided in Appendix A. The maximum physical sizes of each component corresponding to the linking length of 0.138 and 0.487 are summarized in Table 2.

Linking length	$\theta(l_{\text{orbit}}, b_{\text{orbit}})$ (deg)	a (kpc)	e	l_{apo} (deg)
0.138	7.36	1.46	0.04	13.90
0.487	25.99	5.17	0.16	49.05

Table 2. The maximum physical sizes of each component corresponding to the linking lengths of 0.138 and 0.487.

4 RESULTS

As described in Section 3, we apply the FoF algorithm to search for substructures in the IoM space. We ultimately identify 47 groups containing a total of 1,597 M giant stars. By comparing their spatial distribution, kinematics, dynamics, and chemical properties with those of known substructures, we find that the groups mainly belong to the Sgr stream (Belokurov et al. 2014; Hernitschek et al. 2017; Yang et al. 2019b), Galactic Anticenter Substructure (GASS) (Li et al. 2021), GES (Belokurov et al. 2018; Naidu et al. 2020),

Splash (Belokurov et al. 2020), and the high- α disk (Naidu et al. 2020; Tang et al. 2024). Figure 3 shows the distribution of these substructures in the Galactic coordinate system (l , b) and the energy-angular momentum (L_z - E) space. Additionally, we find two new groups which are not associated with any known substructures. In the following, we will provide a detailed explanation of these substructures. Table 3 shows the orbital parameters of all identified substructures.

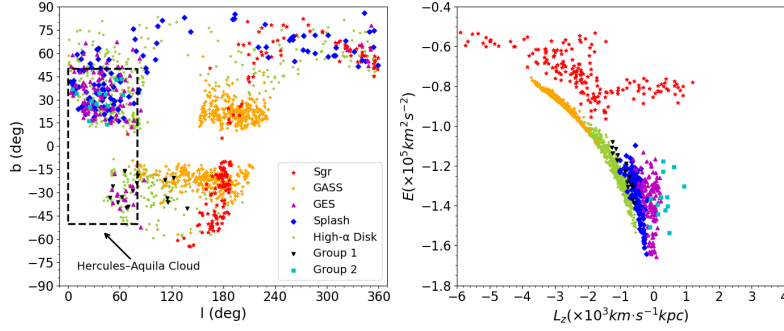


Figure 3. The distributions of groups associated with known substructures in the Galactic coordinate system and the L_z - E plane. The figure includes the known substructures Sgr (red pentagram), GASS (orange plus), GES (purple triangle), Splash (blue diamond), and High- α Disk (yellow-green dots), as well as two possible new substructures: Group 1 (black downward triangle) and Group 2 (cyan square). The black dashed areas in the left panel indicate the location of the Hercules–Aquila Cloud as defined by Belokurov et al. (2007).

4.1 The Sagittarius stream

The Sgr stream, the most prominent substructure in the Galactic halo, exhibits a growing population of spectroscopically confirmed member stars. This expanded census facilitates a comprehensive investigation of the dynamical interaction between the Sagittarius dwarf spheroidal galaxy (Sgr dSph) and the Milky Way (Ibata et al. 1994; Yanny et al. 2000; Ibata et al. 2001; Belokurov et al. 2006; Carlin et al. 2018; Li et al. 2019; Yang et al. 2019b). By comparing our groups with previous observational Sgr members (Belokurov et al. 2014; Hernitschek et al. 2017; Yang et al. 2019b), we identify three groups (182 stars) associated with the Sgr stream: one group (67 stars) in the Sgr leading arm, one group (105 stars) in the Sgr trailing arm, and one group (10 stars) in the Sgr debris. We cross-matched the Sgr sample with APOGEE DR17 and obtained 19 stars with reliable $[M/H]$ and $[\alpha/M]$ measurements.

Qiu et al. (2023) estimated the distances of M giant stars based on their intrinsic color index, metallicity, and extinction. However, Li et al. (2016a) suggested that the distances of M giants are not solely determined by these parameters but are also strongly affected by the star formation history of their host system. Consequently, compared to Sgr member stars identified using other stellar tracers, the distances derived by Qiu et al. (2023) for the Sgr stream are noticeably underestimated (Belokurov et al. 2014; Hernitschek et al. 2017; Yang et al. 2019b). To address this, we correct the distances of the identified Sgr member stars using the color–absolute magnitude relation derived from Li et al. (2016a). Figure 4 presents a comparison of our Sgr stream sample with other observational data (Belokurov et al. 2014; Hernitschek et al. 2017; Yang et al. 2019b) across the $(\tilde{A}_\odot, V_{\text{los}})$, (\tilde{A}_\odot, d) , and $(X_{\text{gc}}, Z_{\text{gc}})$ spaces. The velocities and distances of our identified Sgr members show excellent agreement with those from other observational studies.

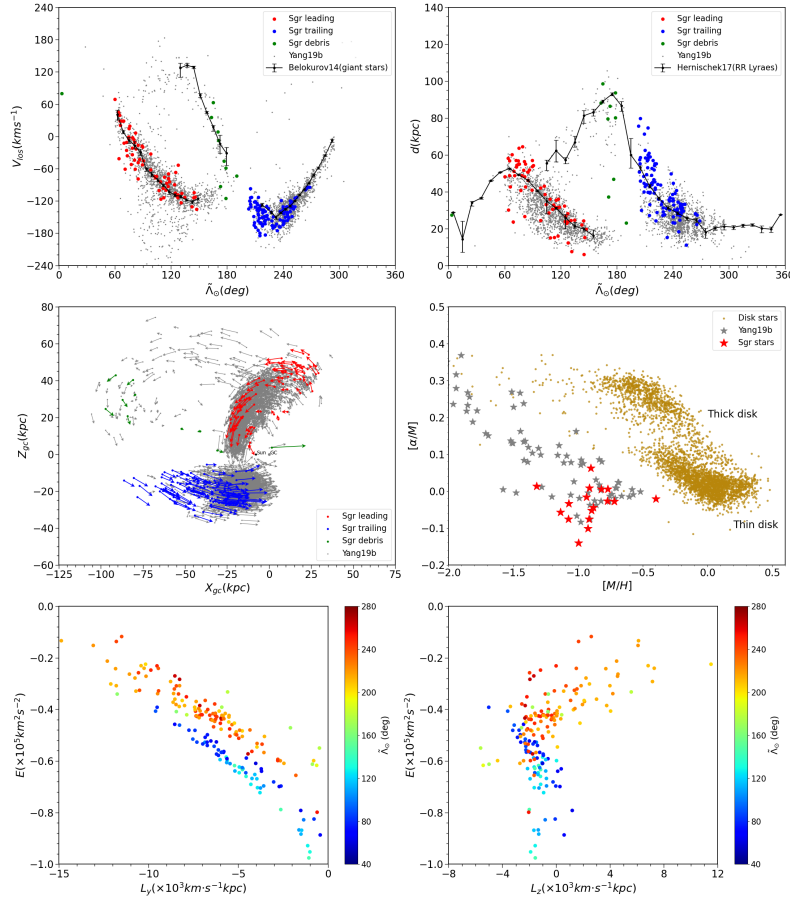


Figure 4. The distributions of the Sgr members in the \tilde{L}_O - V_{los} , \tilde{L}_O - d , X_{gc} - Z_{gc} , $[M/H]$ - $[\alpha/M]$, L_z - E , and L_y - E planes. \tilde{L}_O is the longitude in the Sgr coordinate system and the definition is the same as that in Belokurov et al. (2014). The red, blue, and green points in the figure represent members of the Sgr leading arm, trailing arm, and debris, respectively, while the gray points represent the observational sample from Yang et al. (2019b). The black points with error bars in the upper-left panel represent the giant stars from Belokurov et al. (2014). The black points with error bars in the upper-right panel represent the RR Lyrae stars from Hernitschek et al. (2017). Arrows in the middle-left panel indicate the direction and amplitude of the velocity in the X_{gc} - Z_{gc} plane. The middle-right panel shows a comparison of our Sgr stars (red stars) with Galactic disk stars (yellow points) and Sgr stars from Yang et al. (2019b) in the $[\alpha/M]$ vs. $[M/H]$ space. All $[M/H]$ and $[\alpha/M]$ measurements are taken from APOGEE DR17. The lower two panels show energy-angular momentum distribution and the color indicates the \tilde{L}_O value.

From the spatial distribution in the X_{gc} - Z_{gc} plane and energy-angular momentum distribution shown in Figure 4, the traditionally identified leading stream appears to consist of two distinct orbital components: one part vertically passes through the Galactic disk, while the other part runs almost parallel to the disk. In the energy-angular momentum distribution, we also see that the leading members are clearly divided into dark blue and light blue groups based on their \tilde{L}_O values. Further work will focus on a more in-depth orbital analysis by incorporating different types of Sgr member stars.

Additionally, in the middle-right panel of Figure 4, our Sgr stars exhibit a distribution sequence similar to that of the Sgr stars identified in K giants, M giants and BHBs from Yang et al. (2019b), characterized by lower $[\alpha/M]$ abundances compared to Galactic disk stars at high metallicity. This chemical evolution pattern is consistent with Milky Way dwarf galaxies (Venn et al. 2012; Lemasle et al. 2014; Yang et al. 2019b).

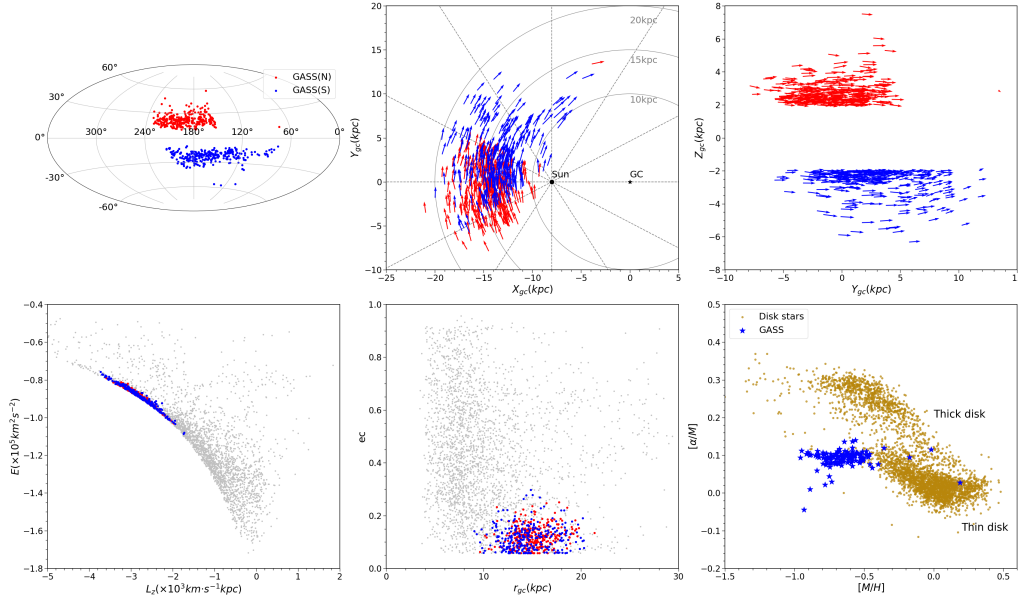


Figure 5. Distribution of our GASS members in (l, b) , (X_{gc}, Y_{gc}) , (Y_{gc}, Z_{gc}) , (L_z, E) , (r_{gc}, ec) , and $([M/H], [\alpha/M])$ spaces. The blue and red points represent the members in the northern and southern hemispheres respectively. The silver points represent all M giant stars. In the second and third panels of the upper row, arrows indicate the direction and amplitude of the velocity in the X_{gc} - Y_{gc} and Y_{gc} - Z_{gc} planes. In the third panel of the lower row, the blue stars represent 122 GASS M giants, while the yellow points represent the disk stars from Yang et al. (2019b). All $[M/H]$ and $[\alpha/M]$ measurements are taken from APOGEE DR17.

4.2 The Galactic Anticenter Substructure

The GASS is a substructure located at low Galactic latitudes and in the anti-center direction of the Milky Way. Due to their overlapping kinematics and spatial properties, Li et al. (2021) grouped several previously identified anti-center substructures, including Monoceros (Newberg et al. 2002; Li et al. 2012), A13 (Sharma et al. 2010; Li et al. 2017), and the Triangulum-Andromeda cloud (Rocha-Pinto et al. 2004; Deason et al. 2014). Li et al. (2021) obtained a GASS sample containing 589 stars, among which 280 stars are M giants, and suggested that GASS is part of the local metal-poor outer disk of the Milky Way.

By comparing the properties of the GASS with those reported in Li et al. (2021), we identify 11 groups comprising a total of 594 M giant stars associated with the GASS. Among these, 313 stars are located in the northern part of the Galactic disk, and 281 stars reside in the southern part. We cross-matched the GASS sample with APOGEE DR17 and obtained 122 stars with reliable $[M/H]$ and $[\alpha/M]$ measurements. Figure 5 shows the distribution of the GASS members in (l, b) , (X_{gc}, Y_{gc}) , (Y_{gc}, Z_{gc}) , (L_z, E) , and (r_{gc}, ec) spaces, as well as the comparison between GASS and disk stars in the $[M/H]$ - $[\alpha/M]$ planes. In the upper left panel, it can be seen that these members cover a large region at low latitude with a range of $100^\circ < l < 240^\circ$ and $-40^\circ < b < 40^\circ$. In the X_{gc} - Y_{gc} plane, the GASS exhibits a prograde circular orbit. Additionally, in the Y_{gc} - Z_{gc} plane, the GASS has a slight arc motion trend, particularly in the southern hemisphere, consistent with the results of Li et al. (2021). Li et al. (2021) suggested that it could be part of the expected ripple pattern in Xu et al. (2015) and Li et al. (2017). In the L_z - E plane, it is located in an extended narrow region of thin disk stars, but has a higher E and higher L_z value than most of the thin disk population. The r_{gc} -

ec plane shows that the GASS mainly distributes in the range of $r_{gc} = 10$ kpc to 20 kpc, with an orbital eccentricity $ec < 0.2$, indicating its very circular orbit.

In the lower-right panel of Figure 5, the comparison with disk stars shows that GASS has similar α -element abundances to the thin disk, but is more metal-poor than typical thin disk stars. This feature is consistent with the continuation of metal-rich thin disk stars into the outer halo (Haywood et al. 2016; Hayes et al. 2018; Li et al. 2021). Our GASS members share a similar distribution in the $[\alpha/M]$ versus $[M/H]$ space with those identified by Li et al. (2021). According to Li et al. (2021), GASS may have formed in the outer disk region after the thick disk phase, where lower molecular cloud densities resulted in a reduced star formation efficiency compared to the inner disk.

4.3 Gaia-Enceladus-Sausage

The GES is a merger remnant in the Milky Way, formed through a major accretion event with a dwarf galaxy approximately 8–10 billion years ago (Belokurov et al. 2018; Koppelman et al. 2018; Myeong et al. 2018; Haywood et al. 2018; Helmi et al. 2018; Mackereth et al. 2019). Belokurov et al. (2018) first identified the GES based on a large sample of main-sequence stars within ~ 10 kpc, combining data from Gaia DR1 and SDSS. They named it the “Gaia Sausage” due to its distinctive sausage-like distribution in the V_r - V_ϕ plane, where V_r is the radial velocity and V_ϕ is the azimuthal velocity, with $V_\phi \sim 0$ km s $^{-1}$ indicating highly radial orbits. Since its discovery, the GES has been extensively studied (Koppelman et al. 2018; Myeong et al. 2018; Haywood et al. 2018; Helmi et al. 2018; Mackereth et al. 2019; Naidu et al. 2020; Zhao & Chen 2021; Wang et al. 2022; Tang et al. 2024).

In our sample, we identify seven groups belonging to the GES, containing a total of 115 M giant stars. By cross-matching the GES sample with APOGEE DR17, we obtained 11 stars with reliable $[M/H]$ and $[\alpha/M]$ measurements. As shown in Figure 6, our selected GES members are kinematically consistent with the typical GES. In the (L_z, E) plane, the GES shows a vertical bar-like distribution near $L_z \sim 0$ kpc km s $^{-1}$. In the (V_r, V_ϕ) plane, it shows a sausage-like distribution near $V_\phi \sim 0$ km s $^{-1}$ with a broad V_r range and a high eccentricity ($ec > 0.7$).

Zhao & Chen (2021) selected metal-rich Sausage-kinematic (MRSK) stars from the LAMOST DR5 dataset, defined by $[Fe/H] > -0.8$ dex and $-100 < V_\phi < 50$ km s $^{-1}$, then categorized them into low- α and high- α MRSK subgroups using their α -element abundances. In a complementary study, Amarante et al. (2020) conducted a hydrodynamical simulation of a clumpy Milky-Way-like analogue that successfully replicated bimodal disk chemistry with Sausage-like kinematics. Building on the consistency between MRSK stellar properties and these simulations, Zhao & Chen (2021) hypothesized that both low- α and high- α MRSK population originates from the GES progenitor galaxy. They posited that the ancient GES merger introduced gas-rich clouds into the Milky Way during its early evolution, subsequently forming clumps that generated the observed bimodal chemistry through later evolutionary processes.

As demonstrated in the middle-right panel of Figure 6, our metal-rich GES M giants display two distinct α -abundance sequences (high- α vs. low- α), thereby corroborating Zhao & Chen (2021)’s scenario. Furthermore, comparative analysis with Tang et al. (2024)’s GES stars reveals that our M giants trace the GES metallicity extension from metal-poor to metal-rich regimes, strengthening Zhao & Chen (2021)’s

interpretation of MRSK stars as the metal-rich component of the GES. Finally, for our GES sample, the R and $|Z|$ distributions ($2 < R < 12$ kpc; $2 < |Z| < 8$ kpc) align with the metal-rich GES spatial trends reported in Figure 5 of Zhao & Chen (2021).

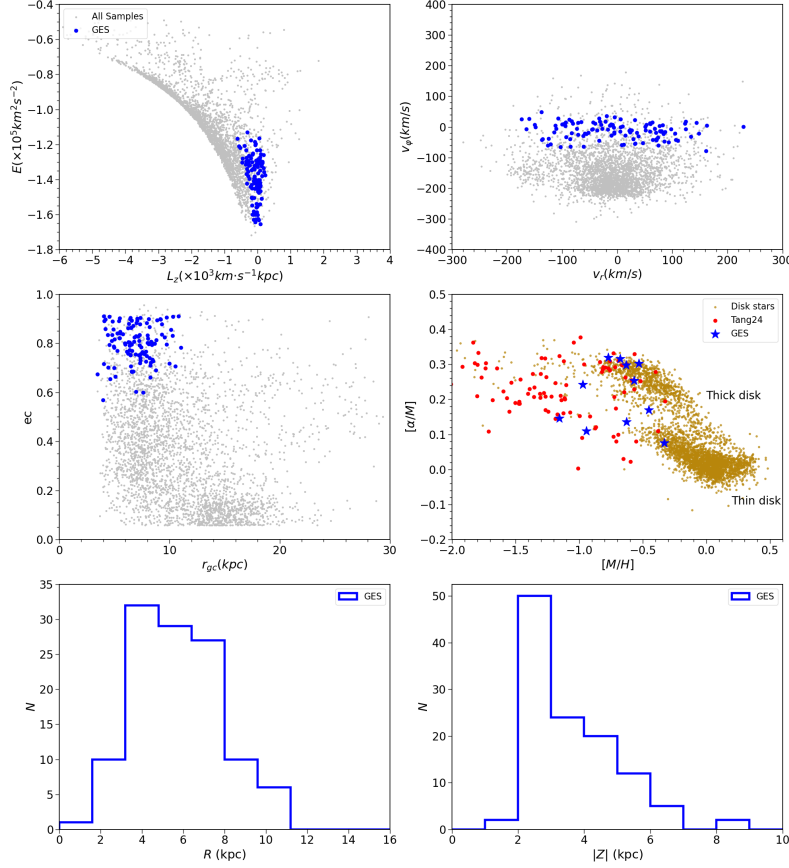


Figure 6. Distribution of the GES in the L_z - E , V_r - V_ϕ , r_{gc} - e_c , and $[M/H]$ - $[\alpha/M]$ planes, as well as histograms of R and $|Z|$. The blue points represent all the selected GES member stars, while the silver points represent all M giant stars. In the middle-right panel, the blue and red star symbols represent the GES M giants from our sample and the GES stars from Tang et al. (2024), respectively. The yellow points represent disk stars from Yang et al. (2019b). All $[M/H]$ and $[\alpha/M]$ measurements are taken from APOGEE DR17. The lower two panels show the histograms of R and $|Z|$ for our GES, respectively.

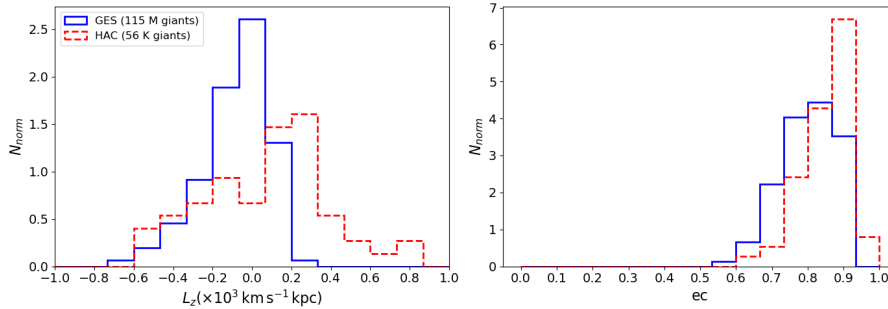


Figure 7. The distribution of the angular momentum (L_z) and eccentricity (e_c) of GES members. The blue solid line traces the distribution of the GES members in our sample, while the red dashed line traces the distribution of HAC K giants from Yang et al. (2019a).

Previous studies (e.g. Li et al. 2016b; Balbinot & Helmi 2021; Wang et al. 2022) have suggested a connection between GES and the Hercules–Aquila Cloud (HAC). Belokurov et al. (2007) first discovered the HAC and suggested that it covers a vast area of the sky, centered at a Galactic longitude of $l \sim 40^\circ$, with Galactic latitude b from -50° to $+50^\circ$. Figure 3 shows that most of our GES member stars are located within the HAC region. Therefore, to explore their connection, we compare the GES with the HAC K-giant sample identified by Yang et al. (2019a). As shown in Figure 7, the GES, similar to the HAC, exhibits high orbital eccentricity and low L_z . The slight deviation between the GES members and HAC K giants in the L_z distribution can be attributed to the insufficient number of M giants. Given similar kinematic properties of GES and HAC, we reach the same conclusion as Wang et al. (2022) that GES and HAC may have similar origins.

4.4 Splash

The existence of the in situ halo in the Milky Way has long been a topic of significant interest. Bonaca et al. (2017) constructed a large sample of high-eccentricity stars with $[\text{Fe}/\text{H}] > -1$ using Gaia DR1 data. Based on chemical abundance analysis and comparisons with numerical simulations, Bonaca et al. (2017) argued that these locally observed metal-rich stars on halo-like orbits were most likely formed within the Galaxy. Subsequent studies based on Gaia DR2 data have also identified stellar populations that exhibit both high orbital eccentricities and thick disk chemical abundance patterns, and have referred to one such component as the “heated thick disc”, interpreted as the in situ halo (Haywood et al. 2018; Di Matteo et al. 2019; Amarante et al. 2020).

In particular, Belokurov et al. (2020) confirmed the existence of a large metal-rich population of stars ($[\text{Fe}/\text{H}] > -0.7$) on highly eccentric orbits ($ec > 0.5$) in the solar neighborhood. Their analysis leveraged Gaia DR2 astrometry and spectroscopic data for bright nearby stars. By analyzing the evolution of kinematics, elemental abundances and stellar ages in the V_ϕ – $[\text{Fe}/\text{H}]$ plane, Belokurov et al. (2020) further proposed that these stars likely originated in the Milky Way’s proto-disk prior to a massive ancient accretion event, such as the GES merger which drastically perturbed their orbits. Thus, this component was named “Splash”. This scenario provides crucial insights into the early dynamical evolution of the Milky Way. Follow-up studies have since characterized Splash stars via their distinct phase-space signatures in the energy–angular momentum space and chemical abundance patterns (Naidu et al. 2020; Bonaca et al. 2020; Myeong et al. 2022; Deepak 2024; Tang et al. 2024).

In this work, we identify seven groups (121 stars) as members of the Splash component and characterize their kinematic and chemical properties, such as high orbital eccentricities ($ec > 0.5$) and thick disk chemistry ($[\text{M}/\text{H}] > -1$ dex) (Belokurov et al. 2020; Naidu et al. 2020; Bonaca et al. 2020; Deepak 2024). By cross-matching the Splash sample with APOGEE DR17, we obtained 23 stars with reliable $[\text{M}/\text{H}]$ and $[\alpha/\text{M}]$ measurements.

As shown in Figure 8, Splash candidates occupy angular momenta $-1 \times 10^3 < L_z < 0 \text{ kpc km s}^{-1}$, yet their L_z values are systematically lower than thick disk stars at matched energies. In the V_r – V_ϕ plane, Splash members predominantly lie above the kinematic boundary $V_\phi \sim -100 \text{ km s}^{-1}$ (Belokurov et al. 2020), distinguishing them from the thick disk. Additionally, their V_r distributions show significantly greater dis-

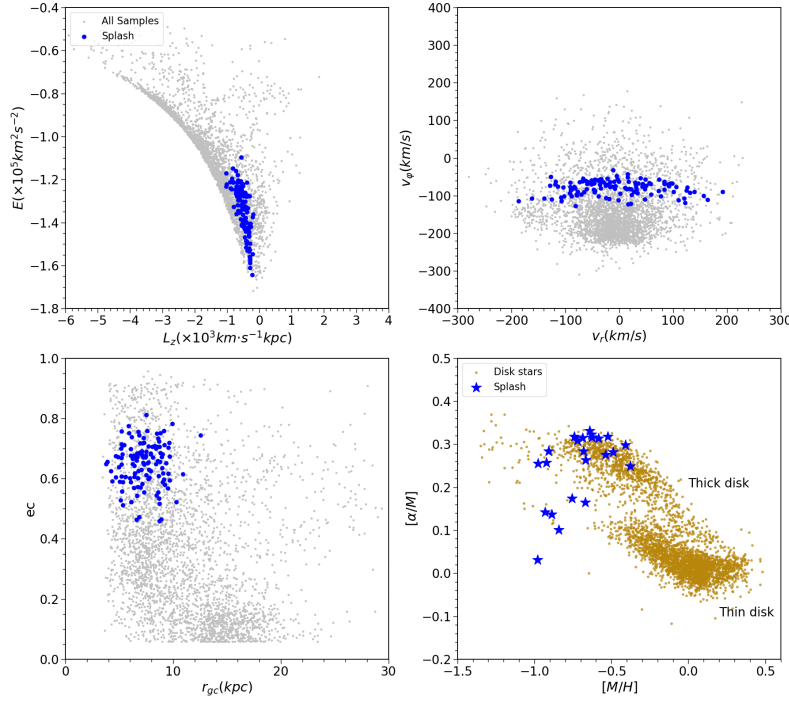


Figure 8. Distribution of the Splash in the L_z - E , V_r - V_ϕ , r_{gc} - ec , and $[M/H]$ - $[\alpha/M]$ planes. The blue points and silver points represent the Splash members and all M giants, respectively. In the bottom-right panel, the blue stars represent 23 Splash M giants, while the yellow points represent the disk stars from Yang et al. (2019b). All $[M/H]$ and $[\alpha/M]$ measurements are taken from APOGEE DR17.

persion compared to the thick disk population. As shown in the lower-left panel of Figure 8, Splash stars exhibit distinctly high orbital eccentricities ($ec > 0.5$), differentiating them from thick disk stars. However, in the chemical plane of $[M/H]$ versus $[\alpha/M]$, the Splash population largely overlaps with the thick disk sequence. These properties of the Splash stars further support the scenario proposed in the previous literature, which suggests that Splash stars formed in the Milky Way’s high- α proto-disk and were subsequently heated to high-eccentricity orbits by a massive ancient accretion event (Bonaca et al. 2017; Haywood et al. 2018; Di Matteo et al. 2019; Amarante et al. 2020; Belokurov et al. 2020; Bonaca et al. 2020).

As shown in Figure 6 and 8, our Splash population exhibits higher angular momentum and prograde rotational velocity, as well as lower orbital eccentricity, compared to the GES population. We initially distinguished Splash from GES based on these kinematic characteristics. However, we note that Tang et al. (2024) found a Splash population within the GES stars identified in the IoM space. Additionally, Previous studies have suggested that Splash stars are generally high- α and metal-rich, consistent with the thick disk (Belokurov et al. 2020; Naidu et al. 2020; Bonaca et al. 2020; Deepak 2024). Meanwhile, Zhao & Chen (2021), based on the hydrodynamical simulation results of Amarante et al. (2020), suggested that both low- α and high- α MRSK stars coexist within GES. Therefore, we speculate that a small number of both low- α and high- α GES stars may be present in our Splash sample. This is also supported by the presence of a few low- α stars ($[\alpha/M] < 0.2$ dex) in the $[M/H]$ versus $[\alpha/M]$ plane, as shown in Figure 8.

The kinematic overlap between Splash and GES also implies the presence of dynamical interaction between them. Based on the above information, we suggest that the high-eccentricity, high- α stars may

include both stars originating from the GES and Splash stars that were born in the Milky Way’s high- α proto-disk and later heated onto eccentric orbits due to the GES merger event.

4.5 The High- α Disk

The high- α disk is a chemically distinct stellar population marked by elevated α -element abundances (Edvardsson et al. 1993; Fuhrmann 1998; Chen et al. 2000; Bensby et al. 2003; Adibekyan et al. 2012; Recio-Blanco et al. 2014; Hayden et al. 2015; Carollo et al. 2019; Nissen et al. 2020). Bonaca et al. (2020) selected 4,631 high- α stars with low orbital eccentricities ($e < 0.5$) from 11,000 main-sequence turn-off stars in the H3 Survey, and defined them as the “high- α disk”. Based on analyses of their orbital properties, ages, and elemental abundances, Bonaca et al. (2020) proposed that this stellar population originated in the Milky Way’s high- α proto-disk. Subsequent studies have further identified low-eccentricity, α -enhanced stellar populations as part of the high- α disk component, suggesting that these stars are typically old and formed during the early stages of the Galaxy’s evolution (Naidu et al. 2020; Xiang & Rix 2022; Tang et al. 2024; Xiang et al. 2025).

We identify 17 groups associated with the high- α disk, comprising a total of 557 stars. We cross-matched them with APOGEE DR17 and obtained 83 stars with reliable $[M/H]$ and $[\alpha/M]$ measurements. As illustrated in Figure 9, the high- α disk spans from prograde circular orbits ($L_z \sim -2.5 \times 10^3 \text{ km} \cdot \text{s}^{-1} \cdot \text{kpc}$) to elliptical orbits ($L_z \sim -0.5 \times 10^3 \text{ km} \cdot \text{s}^{-1} \cdot \text{kpc}$) in the L_z - E plane. The azimuthal velocity V_ϕ and orbital eccentricity ec exhibit broad distributions, with V_ϕ ranging from -100 km s^{-1} to -200 km s^{-1} , and ec from 0.1 to 0.5, respectively.

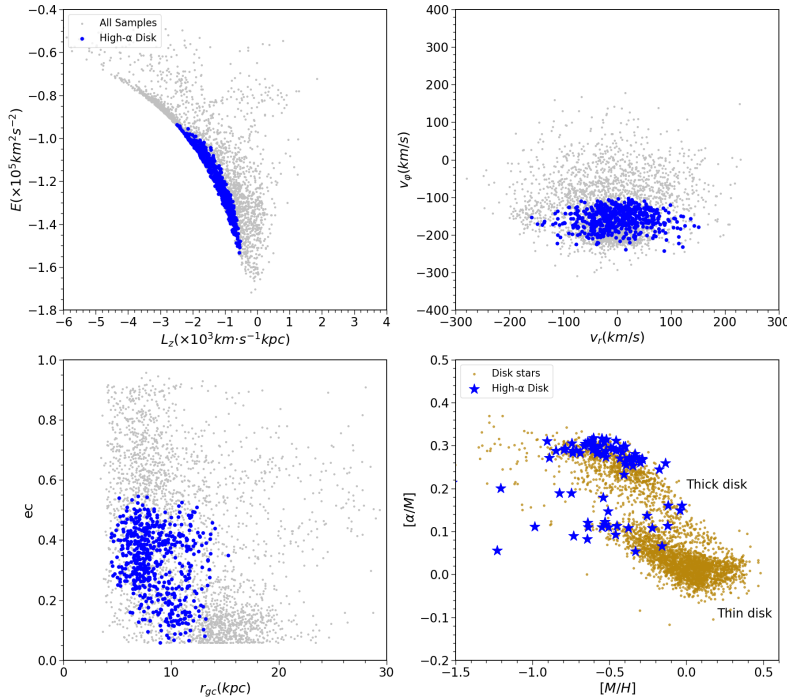


Figure 9. Distribution of high- α disk stars in the L_z - E , V_r - V_ϕ , r_{gc} - ec , and $[M/H]$ - $[\alpha/M]$ planes. The blue points represent high- α disk members, while the silver points represent all M giants. In the bottom-right panel, the blue stars represent 83 high- α disk stars, while the yellow points represent the disk stars from Yang et al. (2019b). All $[M/H]$ and $[\alpha/M]$ measurements are taken from APOGEE DR17.

Additionally, in the $[M/H]$ – $[\alpha/M]$ plane, high- α disk predominantly align with the thick disk sequence. The high rotational velocities, low orbital eccentricities, and thick disk-like chemical abundances collectively indicate that this stellar population formed in situ within the Milky Way’s proto-disk. This result further confirms the scenario proposed by Bonaca et al. (2020), which suggests that stars in the Milky Way initially formed in the high- α proto-disk. A subsequent massive ancient accretion event dynamically heated a fraction of these high- α stars, placing them on high-eccentricity orbits (now identified as the Splash population), while the remaining stars retained disk-like orbits, forming the so-called high- α disk.

Since the clustering analysis primarily relies on orbital parameters, some low- α disk stars with orbital features highly similar to those of the high- α disk population are misclassified into the latter (as shown in the lower right panel of Figure 9). These two populations can be further distinguished by incorporating more α -abundance data.

4.6 Unclassified Groups

In our results, we also identify two groups which cannot be clearly associated with previously known substructures. We designate them as Group 1 and Group 2, containing 15 and 13 stars, respectively. We cross-matched the two groups with APOGEE DR17, and obtained two stars of Group 2 with reliable $[M/H]$ and $[\alpha/M]$ measurements.

Figure 10 illustrates the distribution of these groups in chemodynamical space. For Group 1, the mean z-component of angular momentum is $\langle L_z \rangle = -0.912 \times 10^3 \text{ kpc km s}^{-1}$ and the mean energy is $\langle E \rangle = -1.22 \times 10^5 \text{ km}^2 \text{ s}^{-2}$. In contrast, Group 2 has a mean z-component of angular momentum $\langle L_z \rangle = 0.318 \times 10^3 \text{ kpc km s}^{-1}$, and a mean energy $\langle E \rangle = -1.36 \times 10^5 \text{ km}^2 \text{ s}^{-2}$. In the V_r – V_ϕ plane, Group 1 is centered around $V_\phi = -100 \text{ km s}^{-1}$, while Group 2 exhibits a more dispersed distribution within $0 < V_\phi < 200 \text{ km s}^{-1}$, indicating slight retrograde motion. Additionally, Group 1 has a higher mean orbital eccentricity ($\langle ec \rangle = 0.55$) compared to Group 2 ($\langle ec \rangle = 0.35$).

In the kinematic space, Group 1 exhibits energy-angular momentum distributions and kinematic patterns similar to those of the Splash population. However, it has slightly lower orbital eccentricities and larger galactocentric distances (r_{gc}). Due to the lack of chemical abundance data, we cannot definitively determine the origin of Group 1. Nevertheless, its kinematic and dynamical properties suggest a potential origin in the Galactic disk.

Given its slight retrograde motion, we hypothesize that Group 2 is related to the low-energy retrograde substructure Thamnos (Koppelman et al. 2019a; Naidu et al. 2020), as it shares a relatively low energy $\langle E \rangle = -1.36 \times 10^5 \text{ km}^2 \text{ s}^{-2}$ and eccentricity $\langle ec \rangle = 0.35$. However, as shown in the lower-right panel of Figure 10, two stars in Group 2 with metallicity measurements from APOGEE DR17 are more metal-rich than the classical Thamnos population, which typically has $[Fe/H] < -1.6 \text{ dex}$ (Koppelman et al. 2019a; Naidu et al. 2020). Nevertheless, we do not rule out the possibility that Group 2 represents the metal-rich tail of the Thamnos substructure.

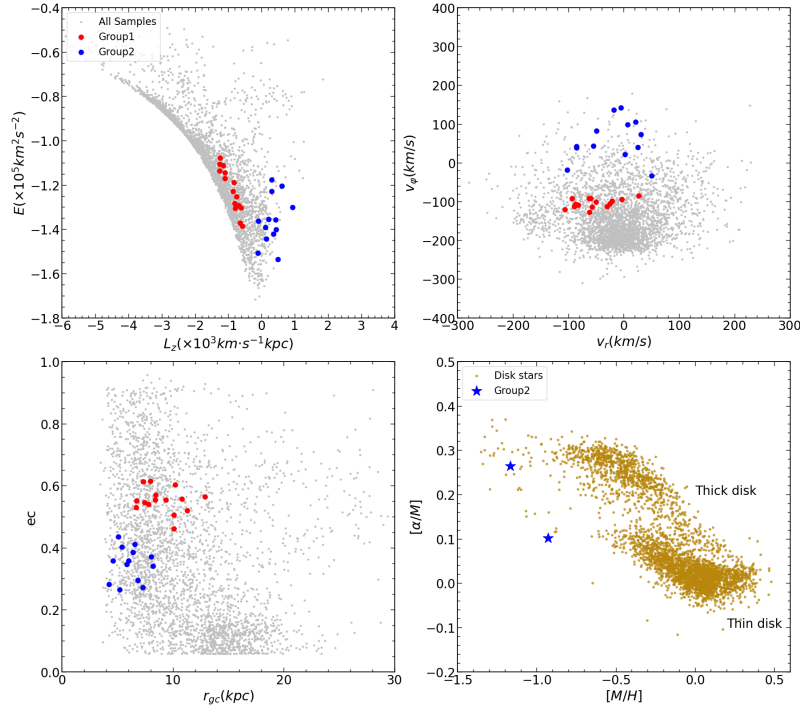


Figure 10. The distribution of the unclassified groups in the chemodynamical space. The red and blue points in the figure represent Group 1 and Group 2, respectively. The silver points represent all M giants. In the bottom-right panel, the blue stars represent stars from Group 2, while the yellow points represent the disk stars from Yang et al. (2019b). All $[M/H]$ and $[\alpha/M]$ measurements are taken from APOGEE DR17.

5 DISCUSSION AND CONCLUSION

In this study, we investigate Galactic substructures using a catalog of M giant stars from LAMOST DR9 low-resolution spectroscopic data (Li et al. (2023)). By combining radial velocities from Li et al. (2023), distances from Qiu et al. (2023), and proper motions from Gaia DR3, we derive the full 6D phase-space information of these stars, including their spatial positions and velocity components. All M giants used for identifying substructure are available in Table 1.

After removing M giant stars with $|Z_{gc}| < 2$ kpc, we apply the FoF clustering algorithm to identify stellar groups with similar orbital properties in the IoM space. This process yields 47 groups containing a total of 1,597 M giant stars. By comparing them with known substructures, we find that these groups primarily correspond to the Sgr stream (182 M giants), GASS (594 M giants), GES (115 M giants), Splash (121 M giants), and the high- α disk (557 M giants). Additionally, two groups cannot be clearly associated with previously known substructures. All orbital parameters of identified groups are listed in Table 3.

The Sgr stream in our sample consists of three components: the Sgr leading arm, the Sgr trailing arm, and Sgr debris. Their velocity and distance distributions are consistent with previous studies. Our analysis reveals that the traditionally defined leading stream consists of two kinematically distinct components, suggesting a more complex orbital structure than previously thought. Further investigation incorporating different types of Sgr member stars is required to better understand this complexity. The chemical abundance pattern of our Sgr member stars, characterized by low $[\alpha/M]$ at high metallicity, aligns with previous findings and supports the chemical evolution trends commonly observed in Milky Way dwarf galaxies (Venn et al. 2012; Lemasle et al. 2014; Yang et al. 2019b).

The GASS in our sample exhibits nearly circular prograde orbits spanning galactocentric distances from 10 to 20 kpc, consistent with the kinematic properties reported by (Li et al. 2021). Chemically, the GASS stars have similar α -element abundances to the thin disk but are comparatively more metal-poor, consistent with the continuation of the metal-rich thin disk population into the outer halo (Haywood et al. 2016; Hayes et al. 2018; Li et al. 2021; Zhang et al. 2022). These characteristics suggest that GASS originated from the disk and indicate a distinct formation and evolutionary history within the Milky Way’s outer disk.

Analysis of the GES member stars reveals kinematic and chemical properties consistent with previous studies, including a bar-like distribution in (L_z, E) space and a sausage-shaped structure in (V_r, V_ϕ) space with high eccentricities. The presence of metal-rich M giants exhibiting a wide range of $[\alpha/M]$ supports the GES origin scenario proposed by Zhao & Chen (2021), in which both the ancient GES merger event brought a gas-rich cloud into the Milky Way at an early epoch, and produced clumps that developed this bimodal chemistry for MRSK stars in later evolution. Furthermore, the spatial and dynamical similarities between our GES members and the HAC suggest a possible common origin, in agreement with the conclusions of Wang et al. (2022).

We identify the Splash component, characterized by their high orbital eccentricities and thick disk-like chemical abundance patterns. Our results demonstrate a clear kinematic distinction from thick disk stars and a similar chemical sequence, confirming the efficiency of our FoF clustering method in recovering Splash members in the IoM space. These findings support the scenario that Splash stars originated in the Milky Way’s high- α proto-disk and were dynamically heated by a massive early accretion event (Bonaca et al. 2017; Haywood et al. 2018; Di Matteo et al. 2019; Amarante et al. 2020; Belokurov et al. 2020; Bonaca et al. 2020). Additionally, the presence of a few low- α stars suggests a possible contamination from the low- α , metal-rich tail of the GES galaxy (Zhao & Chen 2021), highlighting the complex interplay between in-situ and accreted populations. We also identify the high- α disk population, whose high rotational velocities, low orbital eccentricities, and thick disk-like chemical abundance patterns indicate an in situ origin from the Milky Way’s proto-disk.

In addition, we identify two groups which cannot be clearly associated with previously known substructures. Group 1 shows kinematic properties similar to the Splash but with lower orbital eccentricities and larger galactocentric distances, suggesting a possible origin in the Galactic disk. Group 2 shows kinematic consistency with the low-energy retrograde substructure Thamnos (Koppelman et al. 2019a; Naidu et al. 2020), though its higher metallicity suggests it may represent a more metal-rich extension of Thamnos.

Based on the kinematic and chemical properties of the metal-rich M giant stars successfully identified in this study as members of the GES, Splash, and high- α disk components, we confirm the evolutionary scenario of the early Milky Way proposed by previous studies, in which stars in the Milky Way initially formed in the high- α proto-disk. A subsequent massive ancient accretion event dynamically heated a fraction of these high- α stars, placing them on high-eccentricity orbits (now identified as the Splash population), while the remaining stars retained disk-like orbits, forming the so-called high- α disk (Helmi et al. 2018; Belokurov et al. 2020; Bonaca et al. 2020; Zhao & Chen 2021; Chandra et al. 2024). In the future, more precise measurements of their chemical abundances (e.g., $[\alpha/M]$ and $[Fe/H]$) using high-resolution spectroscopic data, along with age estimates, will be crucial in robustly verifying the origin of these M giants

and their role in the GES merger event. This discovery provides new insights into the star formation history of the GES progenitor galaxy and its contribution to the evolution of the Milky Way.

Table 3. Orbital parameters of all Galactic substructures we identified. The first column indicates the stellar substructure affiliation, and the second column represents the LAMOST observation ID.

Substructure	LAMOST	a	ec	l_{or}	b_{or}	l_{apo}	E	L	L_x	L_y	L_z
Sgr stream	270210167	11.78	0.25	227.59	-54.34	47.52	-95226.95	2341	-919.74	-1007.26	-1901.75
Sgr stream	563808192	27.84	0.33	279.15	-14.23	100.35	-65980.43	4770.51	735.31	-4564.55	-1169.49
Sgr stream	814912143	30.28	0.36	283.34	-13.32	99.3	-63337.47	5034.6	1130.96	-4767.55	-1158.31
Sgr stream	660004143	14.77	0.37	224.66	-30.11	28.61	-86717.55	2659.09	-1614.48	-1616.21	-1334.45
Sgr stream	531309081	31.46	0.29	285.95	-17.66	108.47	-62335.35	5393.26	1409.21	-4939.6	-1637.71
Sgr stream	422602068	14.16	0.34	221.21	-29.62	43.01	-88327.87	2624.12	-1699.25	-1503.97	-1298.09
Sgr stream	700501081	32.02	0.31	279.85	-13.93	95.23	-61789.63	5445.59	903.74	-5207.6	-1313.01
Sgr stream	425310085	26.88	0.43	269.53	-9.74	86.26	-66773.76	4298.02	-34.1	-4234.39	-728.34
Sgr stream	502013024	34.04	0.31	283.97	0.22	83.47	-59869.61	5790.92	1401	-5617.93	22.64
Sgr stream	132105073	24.01	0.4	269.08	-18.68	80.35	-70471.15	3974.71	-60.54	-3761.52	-1280.21

(This table is available in its entirety in machine-readable form.)

Acknowledgements We thank the referee for providing a number of helpful suggestions that further refined our work. This work is supported by the National Key Research and Development Program of China No. 2024YFA1611902, the National Natural Science Foundation of China (NSFC) under grants Nos. 12273027 and 12588202, the Innovation Team Funds of China West Normal University under grant No. KCXTD2022-6, CAS Project for Young Scientists in Basic Research under grants Nos. YSBR-062 and YSBR-092, and the Strategic Priority Research Program of Chinese Academy of Sciences under grant No. XDB1160102. We acknowledge the science research grant from the China Manned Space Project with No. CMS-CSST-2025-A11.

Guo Shou Jing Telescope (the Large Sky Area Multi-Object Fiber Spectroscopic Telescope LAMOST) is a National Major Scientific Project built by the Chinese Academy of Sciences. Funding for the project has been provided by the National Development and Reform Commission. LAMOST is operated and managed by the National Astronomical Observatories, Chinese Academy of Sciences.

This work has made use of data from the European Space Agency (ESA) mission Gaia (<https://www.cosmos.esa.int/gaia>), processed by the Gaia Data Processing and Analysis Consortium (DPAC, <https://www.cosmos.esa.int/web/gaia/dpac/consortium>). Funding for the DPAC has been provided by national institutions, in particular the institutions participating in the Gaia Multilateral Agreement.

Appendix A: DETERMINATION OF THE LINKING LENGTH

Considering the normalized weights of the input sample and the characteristic linking lengths of different substructures, the linking length for each group is determined individually (Wang et al. 2022). As the linking length increases, the number of group members grows slowly at first, but a sudden jump occurs at a certain linking length. This jump likely indicates the merging of multiple groups, leading to the combination of several substructures (Zhang et al. 2024). To avoid such cases, we choose the linking length just before the jump by checking the orbital parameter distributions of the group before and after the jump.

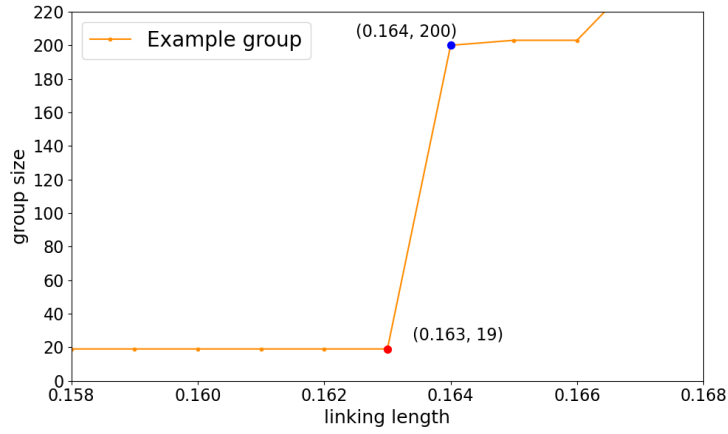


Figure A1. The variation in the number of members of the example group with increasing linking length.

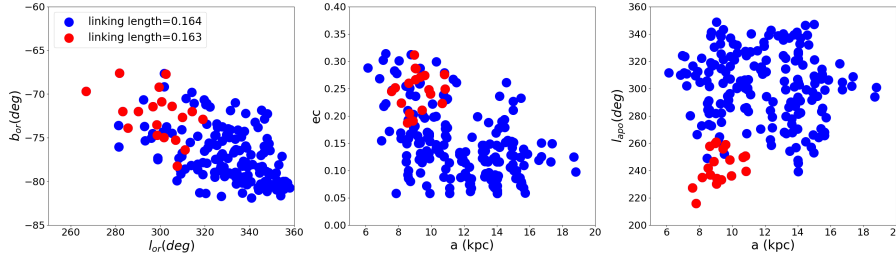




Figure A2. The orbital parameter distribution of the example group members. The red points represent the example group members at a linking length of 0.163, while the blue points represent the example group members at a linking length of 0.164.

Figure A1 illustrates how the number of members in an example group changes with increasing linking length. It shows a significant jump in the number of members when the linking length increases from 0.163 to 0.164. Figure A2 displays the orbital parameter distributions of the group members before and after the jump. It can be seen that at linking length = 0.164, the group becomes unreliable, particularly as the distribution of l_{apo} suggests the presence of multiple substructures. Therefore, we retain this group at linking length = 0.163.


ORCID IDS

Longfei Ding  <https://orcid.org/0009-0007-6842-8117>

Jing Li  <https://orcid.org/0000-0002-4953-1545>

Xiang-Xiang Xue  <https://orcid.org/0000-0002-0642-5689>

Hao Tian  <https://orcid.org/0000-0003-3347-7596>

Zhengzhou Yan  <https://orcid.org/0000-0003-3571-6060>

Gang Zhao  <https://orcid.org/0000-0002-8980-945X>

References

- Abdurro'uf, Accetta, K., Aerts, C., et al. 2022, ApJS, 259, 35, doi: 10.3847/1538-4365/ac4414 4
- Adibekyan, V. Z., Sousa, S. G., Santos, N. C., et al. 2012, A&A, 545, A32, doi: 10.1051/0004-6361/201219401 14

- Ahumada, R., Allende Prieto, C., Almeida, A., et al. 2020, *ApJS*, 249, 3, doi: 10.3847/1538-4365/ab929e 2
- Amarante, J. A. S., Smith, M. C., & Boeche, C. 2020, *MNRAS*, 492, 3816, doi: 10.1093/mnras/staa077 10, 12, 13, 17
- Balbinot, E., & Helmi, A. 2021, *A&A*, 654, A15, doi: 10.1051/0004-6361/202141015 12
- Belokurov, V., Erkal, D., Evans, N. W., Koposov, S. E., & Deason, A. J. 2018, *MNRAS*, 478, 611, doi: 10.1093/mnras/sty982 2, 6, 10
- Belokurov, V., Sanders, J. L., Fattahi, A., et al. 2020, *MNRAS*, 494, 3880, doi: 10.1093/mnras/staa876 2, 7, 12, 13, 17
- Belokurov, V., Zucker, D. B., Evans, N. W., et al. 2006, *ApJ*, 642, L137, doi: 10.1086/504797 7
- Belokurov, V., Evans, N. W., Bell, E. F., et al. 2007, *ApJ*, 657, L89, doi: 10.1086/513144 7, 12
- Belokurov, V., Koposov, S. E., Evans, N. W., et al. 2014, *MNRAS*, 437, 116, doi: 10.1093/mnras/stt1862 6, 7, 8
- Bensby, T., Feltzing, S., & Lundström, I. 2003, *A&A*, 410, 527, doi: 10.1051/0004-6361:20031213 14
- Binney, J. 2012, *MNRAS*, 426, 1324, doi: 10.1111/j.1365-2966.2012.21757.x 2
- Binney, J., & Tremaine, S. 2008, *Galactic Dynamics: Second Edition* 2
- Bonaca, A., Conroy, C., Wetzel, A., Hopkins, P. F., & Kereš, D. 2017, *ApJ*, 845, 101, doi: 10.3847/1538-4357/aa7d0c 12, 13, 17
- Bonaca, A., Conroy, C., Cargile, P. A., et al. 2020, *ApJ*, 897, L18, doi: 10.3847/2041-8213/ab9caa 2, 12, 13, 14, 15, 17
- Carlin, J. L., Sheffield, A. A., Cunha, K., & Smith, V. V. 2018, *ApJ*, 859, L10, doi: 10.3847/2041-8213/aac3d8 7
- Carollo, D., Chiba, M., Ishigaki, M., et al. 2019, *ApJ*, 887, 22, doi: 10.3847/1538-4357/ab517c 14
- Chambers, K. C., Magnier, E. A., Metcalfe, N., et al. 2016, *arXiv e-prints*, arXiv:1612.05560, doi: 10.48550/arXiv.1612.05560 2
- Chandra, V., Semenov, V. A., Rix, H.-W., et al. 2024, *ApJ*, 972, 112, doi: 10.3847/1538-4357/ad5b60 17
- Chen, Y. Q., Nissen, P. E., Zhao, G., Zhang, H. W., & Benoni, T. 2000, *A&AS*, 141, 491, doi: 10.1051/aas:2000124 14
- Deason, A. J., Belokurov, V., Hamren, K. M., et al. 2014, *MNRAS*, 444, 3975, doi: 10.1093/mnras/stu1764 9
- Deepak. 2024, *Journal of Astrophysics and Astronomy*, 45, 25, doi: 10.1007/s12036-024-10011-1 12, 13
- Di Matteo, P., Haywood, M., Lehnert, M. D., et al. 2019, *A&A*, 632, A4, doi: 10.1051/0004-6361/201834929 12, 13, 17
- Edvardsson, B., Andersen, J., Gustafsson, B., et al. 1993, *A&A*, 275, 101 14
- Feuillet, D. K., Sahlholdt, C. L., Feltzing, S., & Casagrande, L. 2021, *MNRAS*, 508, 1489, doi: 10.1093/mnras/stab2614 2

- Fuhrmann, K. 1998, *A&A*, 338, 161–14
- Gaia Collaboration, Vallenari, A., Brown, A. G. A., et al. 2023, *A&A*, 674, A1, doi: 10.1051/0004-6361/202243940 2, 4
- Hayden, M. R., Bovy, J., Holtzman, J. A., et al. 2015, *ApJ*, 808, 132, doi: 10.1088/0004-637X/808/2/132 14
- Hayes, C. R., Majewski, S. R., Hasselquist, S., et al. 2018, *ApJ*, 859, L8, doi: 10.3847/2041-8213/aac38c 10, 17
- Haywood, M., Di Matteo, P., Lehnert, M. D., et al. 2018, *ApJ*, 863, 113, doi: 10.3847/1538-4357/aad235 2, 10, 12, 13, 17
- Haywood, M., Lehnert, M. D., Di Matteo, P., et al. 2016, *A&A*, 589, A66, doi: 10.1051/0004-6361/201527567 10, 17
- Helmi, A. 2020, *ARA&A*, 58, 205, doi: 10.1146/annurev-astro-032620-021917 2
- Helmi, A., Babusiaux, C., Koppelman, H. H., et al. 2018, *Nature*, 563, 85, doi: 10.1038/s41586-018-0625-x 2, 10, 17
- Hernitschek, N., Sesar, B., Rix, H.-W., et al. 2017, *ApJ*, 850, 96, doi: 10.3847/1538-4357/aa960c 6, 7, 8
- Horta, D., Schiavon, R. P., Mackereth, J. T., et al. 2023, *MNRAS*, 520, 5671, doi: 10.1093/mnras/stac3179 2
- Ibata, R., Irwin, M., Lewis, G. F., & Stolte, A. 2001, *ApJ*, 547, L133, doi: 10.1086/318894 7
- Ibata, R., Malhan, K., Martin, N., et al. 2021, *ApJ*, 914, 123, doi: 10.3847/1538-4357/abfcc2 2
- Ibata, R. A., Gilmore, G., & Irwin, M. J. 1994, *Nature*, 370, 194, doi: 10.1038/370194a0 7
- Kerr, F. J., & Lynden-Bell, D. 1986, *MNRAS*, 221, 1023, doi: 10.1093/mnras/221.4.1023 4
- Koppelman, H., Helmi, A., & Veljanoski, J. 2018, *ApJ*, 860, L11, doi: 10.3847/2041-8213/aac882 10
- Koppelman, H. H., Helmi, A., Massari, D., Price-Whelan, A. M., & Starkenburg, T. K. 2019a, *A&A*, 631, L9, doi: 10.1051/0004-6361/201936738 2, 5, 15, 17
- Koppelman, H. H., Helmi, A., Massari, D., Roelenga, S., & Bastian, U. 2019b, *A&A*, 625, A5, doi: 10.1051/0004-6361/201834769 5
- Lemasle, B., de Boer, T. J. L., Hill, V., et al. 2014, *A&A*, 572, A88, doi: 10.1051/0004-6361/201423919 8, 16
- Li, J., Newberg, H. J., Carlin, J. L., et al. 2012, *ApJ*, 757, 151, doi: 10.1088/0004-637X/757/2/151 9
- Li, J., Smith, M. C., Zhong, J., et al. 2016a, *ApJ*, 823, 59, doi: 10.3847/0004-637X/823/1/59 7
- Li, J., FELLOW, L., Liu, C., et al. 2019, *ApJ*, 874, 138, doi: 10.3847/1538-4357/ab09ef 3, 7
- Li, J., Xue, X.-X., Liu, C., et al. 2021, *ApJ*, 910, 46, doi: 10.3847/1538-4357/abd9bf 2, 3, 5, 6, 9, 10, 17
- Li, J., Long, L., Zhong, J., et al. 2023, *ApJS*, 266, 4, doi: 10.3847/1538-4365/acc395 3, 16
- Li, T. S., Balbinot, E., Mondrik, N., et al. 2016b, *ApJ*, 817, 135, doi: 10.3847/0004-637X/817/2/135 12

- Li, T. S., Sheffield, A. A., Johnston, K. V., et al. 2017, *ApJ*, 844, 74, doi: 10.3847/1538-4357/aa7a0d 9
- Mackereth, J. T., Schiavon, R. P., Pfeffer, J., et al. 2019, *MNRAS*, 482, 3426, doi: 10.1093/mnras/sty2955 10
- Malhan, K. 2022, *ApJ*, 930, L9, doi: 10.3847/2041-8213/ac67da 2, 5
- Malhan, K., & Rix, H.-W. 2024, *ApJ*, 964, 104, doi: 10.3847/1538-4357/ad1885 2, 5
- Massari, D., Koppelman, H. H., & Helmi, A. 2019, *A&A*, 630, L4, doi: 10.1051/0004-6361/201936135 2, 5
- Mateu, C. 2023, *MNRAS*, 520, 5225, doi: 10.1093/mnras/stad321 2
- Myeong, G. C., Belokurov, V., Aguado, D. S., et al. 2022, *ApJ*, 938, 21, doi: 10.3847/1538-4357/ac8d68 12
- Myeong, G. C., Evans, N. W., Belokurov, V., Sanders, J. L., & Koposov, S. E. 2018, *ApJ*, 863, L28, doi: 10.3847/2041-8213/aad7f7 2, 10
- Myeong, G. C., Vasiliev, E., Iorio, G., Evans, N. W., & Belokurov, V. 2019, *MNRAS*, 488, 1235, doi: 10.1093/mnras/stz1770 2
- Naidu, R. P., Conroy, C., Bonaca, A., et al. 2020, *ApJ*, 901, 48, doi: 10.3847/1538-4357/abaef4 2, 5, 6, 7, 10, 12, 13, 14, 15, 17
- Necib, L., Ostdiek, B., Lisanti, M., et al. 2020, *Nature Astronomy*, 4, 1078, doi: 10.1038/s41550-020-1131-2 2
- Newberg, H. J., & Carlin, J. L., eds. 2016, *Astrophysics and Space Science Library*, Vol. 420, *Tidal Streams in the Local Group and Beyond*, doi: 10.1007/978-3-319-19336-6 2
- Newberg, H. J., Yanny, B., Rockosi, C., et al. 2002, *ApJ*, 569, 245, doi: 10.1086/338983 9
- Nissen, P. E., Christensen-Dalsgaard, J., Mosumgaard, J. R., et al. 2020, *A&A*, 640, A81, doi: 10.1051/0004-6361/202038300 14
- Ollongren, A. 1965, *ARA&A*, 3, 113, doi: 10.1146/annurev.aa.03.090165.000553 2
- Qiu, D., Tian, H., Li, J., et al. 2023, *Research in Astronomy and Astrophysics*, 23, 055008, doi: 10.1088/1674-4527/acc153 3, 7, 16
- Recio-Blanco, A., de Laverny, P., Kordopatis, G., et al. 2014, *A&A*, 567, A5, doi: 10.1051/0004-6361/201322944 14
- Reid, M. J. 1993, *ARA&A*, 31, 345, doi: 10.1146/annurev.aa.31.090193.002021 4
- Rix, H.-W., Chandra, V., Andrae, R., et al. 2022, *ApJ*, 941, 45, doi: 10.3847/1538-4357/ac9e01 2
- Rocha-Pinto, H. J., Majewski, S. R., Skrutskie, M. F., Crane, J. D., & Patterson, R. J. 2004, *ApJ*, 615, 732, doi: 10.1086/424585 9
- Roederer, I. U., Hattori, K., & Valluri, M. 2018, *AJ*, 156, 179, doi: 10.3847/1538-3881/aadd9c 5
- Schönrich, R., Binney, J., & Dehnen, W. 2010, *MNRAS*, 403, 1829, doi: 10.1111/j.1365-2966.2010.16253.x 4
- Sharma, S., Johnston, K. V., Majewski, S. R., et al. 2010, *ApJ*, 722, 750, doi: 10.1088/0004-637X/722/1/750 9
- Skrutskie, M. F., Cutri, R. M., Stiening, R., et al. 2006, *AJ*, 131, 1163, doi: 10.1086/498708 2

- Sun, S., Wang, F., Zhang, H., et al. 2024, arXiv e-prints, arXiv:2411.13122, doi: 10.48550/arXiv.2411.13122 2, 6
- Tang, X.-Z., Zhao, J.-K., Yang, Y., et al. 2024, *ApJ*, 965, 62, doi: 10.3847/1538-4357/ad3240 2, 5, 7, 10, 11, 12, 13, 14
- Tian, H., Liu, C., Luo, C., Xue, X.-X., & Yang, Y. 2024, *ApJ*, 965, 10, doi: 10.3847/1538-4357/ad2c06 2
- Venn, K. A., Shetrone, M. D., Irwin, M. J., et al. 2012, *ApJ*, 751, 102, doi: 10.1088/0004-637X/751/2/102 8, 16
- Wang, F., Zhang, H. W., Xue, X. X., et al. 2022, *MNRAS*, 513, 1958, doi: 10.1093/mnras/stac874 2, 5, 6, 10, 12, 17, 18
- Xiang, M., & Rix, H.-W. 2022, *Nature*, 603, 599, doi: 10.1038/s41586-022-04496-5 14
- Xiang, M., Rix, H.-W., Yang, H., et al. 2025, *Nature Astronomy*, 9, 101, doi: 10.1038/s41550-024-02382-w 14
- Xu, Y., Newberg, H. J., Carlin, J. L., et al. 2015, *ApJ*, 801, 105, doi: 10.1088/0004-637X/801/2/105 9
- Yan, H., Li, H., Wang, S., et al. 2022, *The Innovation*, 3, 100224, doi: 10.1016/j.xinn.2022.100224 2
- Yang, C., Xue, X.-X., Li, J., et al. 2019a, *ApJ*, 880, 65, doi: 10.3847/1538-4357/ab2462 2, 11, 12
- . 2019b, *ApJ*, 886, 154, doi: 10.3847/1538-4357/ab48e2 2, 3, 4, 5, 6, 7, 8, 9, 11, 13, 14, 16
- Yanny, B., Newberg, H. J., Kent, S., et al. 2000, *ApJ*, 540, 825, doi: 10.1086/309386 7
- York, D. G., Adelman, J., Anderson, John E., J., et al. 2000, *AJ*, 120, 1579, doi: 10.1086/301513 2
- Yuan, Z., Chang, J., Beers, T. C., & Huang, Y. 2020, *ApJ*, 898, L37, doi: 10.3847/2041-8213/aba49f 2
- Zhang, B., Li, J., Yang, F., et al. 2021, *ApJS*, 256, 14, doi: 10.3847/1538-4365/ac0834 3
- Zhang, R., Matsuno, T., Li, H., et al. 2024, *ApJ*, 966, 174, doi: 10.3847/1538-4357/ad31a6 2, 6, 18
- Zhang, Z., Shi, W. B., Chen, Y. Q., et al. 2022, *ApJ*, 933, 151, doi: 10.3847/1538-4357/ac7231 17
- Zhao, G., & Chen, Y. 2021, *Science China Physics, Mechanics, and Astronomy*, 64, 239562, doi: 10.1007/s11433-020-1645-5 2, 10, 11, 13, 17
- Zhao, G., Zhao, Y.-H., Chu, Y.-Q., Jing, Y.-P., & Deng, L.-C. 2012, *Research in Astronomy and Astrophysics*, 12, 723, doi: 10.1088/1674-4527/12/7/002 2